Pharmaceutica Analytica Acta

Amalanathana et al., Pharm Anal Acta 2016, 7:8
DOI: 10.4172/2153-2435.1000504

Research Article Open Access

Infrared Spectral Investigations and Ab Initio Computations of Pharmacological Drug Goniofufurone Monoacetate

Amalanathana M[1*], Ushab D[2], Hubert Joec I[3] and Ajithabaid MD[4]

[1]*Department of Physics, Annai Velankanni College, Tholayavattam-629157, Tamil Nadu, India*

[2]*Department of Physics, Women's Christian College, Nagercoil, Tamil Nadu, India*

[3]*Centre for Molecular and Biophysics Research, Department of Physics, Mar Ivanios College, Thiruvananthapuram-695 015, Kerala, India*

[4]*Department of Chemistry, Mahatma Gandhi College, Thiruvananthapuram, Kerala, India*

[*]**Corresponding author:** Amalanathana M, Department of Physics, Annai Velankanni College, Tholayavattam-629157, Tamil Nadu, India, Tel: +91-9940347178; E-mail: nathan.amalphysics@gmail.com

Received date: July 22, 2016; **Accepted date:** August 27, 2016; **Published date:** August 30, 2016

Abstract

Infrared spectra and Ab initio computation of molecule Goniofufurone monoacetate (GMA) has been analyzed. The equilibrium geometry, bonding features and harmonic vibrational frequencies of GMA have been investigated with the help of B3LYP density functional theory (DFT) method. Potential energy surface (PES) scan studies have also been carried out by Ab initio calculations using DFT level. The natural bond orbital (NBO) analysis confirms the occurrence of strong intramolecular hydrogen bonding in the molecule.

Keywords: FT-IR; DFT; NBO; PES; Hyper-conjugation

Introduction

As a part of the continuing programme for the isolation of bioactive principles from *Goniothalamus* spp., Goniofufurone monoacetate (GMA) is isolated from the leaves of *Goniothalamus wynaadensis* Bedd.(Annonaceae) [1,2]. The structure of the compound was established with the help of IR, NMR and single crystal X-ray studies [3-5]. During the past decade, the density functional theory (DFT) has emerged as a powerful tool in studying vibrational spectra of fairly large molecules, and is accepted by the Ab initio quantum chemical community as a popular method for the computation of molecular structure, vibrational frequencies and energies of chemical reaction [6]. The present investigation aims to understand the structural and bonding features and molecular information such as electronic delocalization, hyper-conjugation and intramolecular charge transfer of the molecule, GMA using DFT calculations along with FT-IR spectral analysis. The change in electron density (ED) in the σ^* antibonding orbitals and E(2) energies has been calculated by natural bond orbital (NBO) analysis. The potential energy surface scan (PES) values and the thermodynamical parameters of the GMA molecule were calculated and analyzed. From the molecular orbital analysis the Highest molecular orbital (HOMO) and Lowest unoccupied molecular orbital (LUMO) energies of the GMA molecules are calculated and analyzed.

Methods

Theoretical

The quantum chemical computations of GMA has been performed using Gaussian '03 program package [7] at the Becke3-Lee-Yang-Parr (B3LYP) level [8,9] with standard 6-31G(d) basis set [10]. Subsequently, the harmonic frequencies and infrared intensities were calculated. The computed optimized geometry and the corresponding parameters are confirmed to be a minimum energy conformation. The computed wavenumbers were scaled by an empirical scaling factor of 0.9613 [11] to fit with the experimental wavenumbers, which accounts for systematic errors caused by basis set incompleteness, neglect of electron correlation and vibrational anharmonicity.

Experimental

The plant material was collected from the Wynaad hills of Kerala, India during December 2005 and was identified by TBGRI, Palode where a voucher specimen has been deposited. Shade dried leaf powder (500) gm was extracted with ethyl alcohol in a soxhlet. 24 gm of gummy residue was obtained. 20 g of it was chromatographed on a glass column (40 mm×80 cm) using silica gel (100-200 mesh). Elution was done with hexane–ethyl acetate mixtures. 50 mL fractions were collected and were analyzed by TLC in glass plates coated with silica gel. Iodine vapor was used as the detector. The compound was obtained as white needles (m.p.186°C) from 40% ethyl acetate–hexane fractions.

The FT-IR spectrum of GMA was recorded in the region 4000-400 cm^{-1}, with samples in the KBr pellet, using Nicolet Magna 560 FT-IR spectrometer. The resolution of the spectrum is 4 cm^{-1}.

Results and Discussions

Optimized geometry

The optimized structure is shown in Figure 1 and the corresponding parameters are given in Table 1. From the optimized geometry the presence of a five-membered lactone ring fused to a furan ring [at the 2,3-position (C_{15} and C_{16})] imposes some conformational rigidity on this compound. The values of relevant torsion angles C_{15}-C_{16}-C_{21}-O_{23}= -6.9125°, C_{15}-C_{21}-C_{22}-O_{23}= 2.6337°, indicate that the five-membered lactone ring adopts the 2E conformation which is

significantly deformed (twisted on C_{15}-C_{16} bond) adopting the shape which is very close to the $^{C\text{-}5}T_{C\text{-}1}$ conformation [12]. The value of C_{12}-C_{13} (1.498 Å), C_{16}-C_{17} (1.492 Å), C_{21}-C_{22} (1.468 Å) and C_3-C_{12} (1.523 Å) are larger than the other C-C bonds, which shows the conjugation of electron donor oxygen to the acceptor carbon atom through the double bond carbon. The increase in C_{15}-C_{21}-H_{32} (132.5°) and C_{21}-C_{22}-O_{33} (129.8°) bond angles also supports this effect. The variation of C-O bond lengths C_{13}-O_{14} (1.252 Å), C_{17}-O_{19} (1.394 Å), C_{12}-O_{25} (1.395 Å) and C_{22}-O_{33} (1.366 Å) is due to different environment of oxygen atom in GMA molecule.

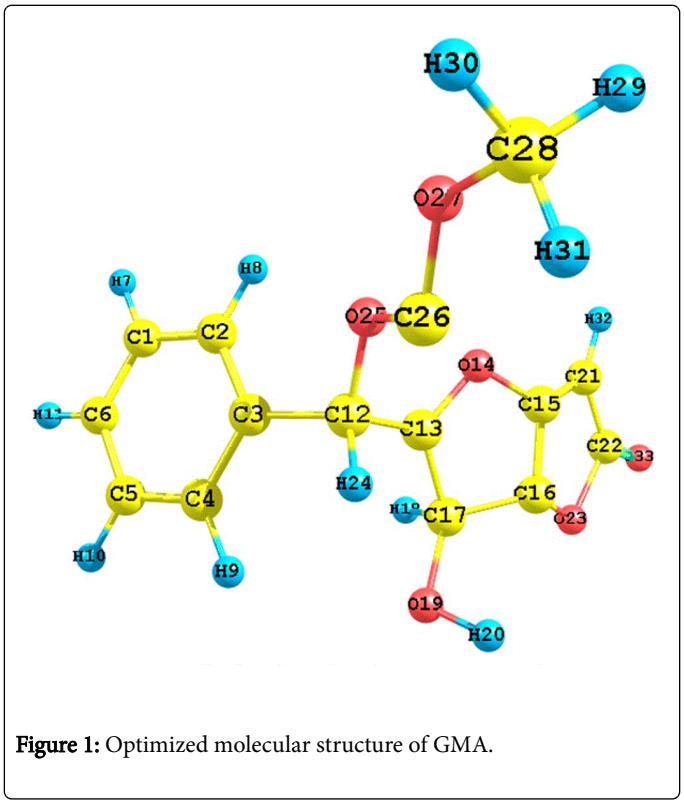

Figure 1: Optimized molecular structure of GMA.

Bond length	Value (Å)	Bond angle	Value (°)	Dihedral angle	Value (°)
C_1-C_2	1.384	C_1-C_2-C_3	119.7	C_1-C_2-C_3-C_4	0.566
C_2-C_3	1.389	C_2-C_3-C_4	120.2	C_2-C_3-C_4-C_5	-0.289
C_3-C_4	1.388	C_3-C_4-C_5	119.9	C_3-C_4-C_5-C_6	-0.061
C_4-C_5	1.385	C_4-C_5-C_6	120	C_1-C_2-C_3-H_7	179.559
C_5-C_6	1.386	C_6-C_1-H_7	120.2	C_6-C_1-C_2-H_8	-179.324
C_1-H_7	1.075	C_1-C_2-H_8	120.2	C_2-C_3-C_4-H_9	179.31
C_2-H_8	1.074	C_3-C_4-H_9	120.1	C_3-C_4-C_5-H_10	-179.809
C_4-H_9	1.075	C_4-C_5-H_{10}	119.7	C_2-C_1-C_6H_{11}	-179.903
C_5-H_{10}	1.075	C_1-C_6-H_{11}	120	C_1-C_2-C_3-C_{12}	179.046
C_6-H_{11}	1.075	C_2-C_3-C_{12}	120	C_2-C_3-C_{12}-C_{13}	-85.555
C_3-C_{12}	1.523	C_3-C_{12}-C_{13}	107.5	C_3-C_{12}-C_{13}-O_{14}	109.523
C_{12}-C_{13}	1.498	C_{12}-C_{13}-O_{14}	120.4	C_{12}-C_{13}-O_{14}-C_{15}	177.306
C_{13}-O_{14}	1.252	C_{13}-O_{14}-C_{15}	106.4	C_{13}-O_{14}-C_{15}-C_{16}	-17.337
O_{14}-C_{15}	1.423	O_{14}-C_{15}-C_{16}	109.5	O_{14}-C_{15}-C_{16}-C_{17}	29.052
C_{15}-C_{16}	1.382	C_{15}-C_{16}-C_{17}	104.4	C_{15}-C_{16}-C_{17}-H_{18}	85.991
C_{16}-C_{17}	1.492	C_{16}-C_{17}-H_{18}	115.1	C_{15}-C_{16}-C_{17}-O_{19}	-143.986
C_{17}-H_{18}	1.092	C_{16}-C_{17}-O_{19}	118.9	C_{16}-C_{17}-O_{19}-H_{20}	8.88
C_{17}-O_{19}	1.394	C_{17}-O_{19}-C_{20}	106.7	C_{13}-O_{14}-C_{15}-C_{21}	146.003
O_{19}-H_{20}	0.951	O_{14}-C_{15}-C_{21}	133	C_{15}-C_{16}-C_{21}-O_{23}	-6.9125
C_{15}-C_{21}	1.34	C_{15}-C_{21}-C_{22}	102.2	C_{15}-C_{21}-C_{22}-O_{23}	2.6337
C_{21}-C_{22}	1.468	C_{15}-C_{16}-O_{23}	103.5	C_2-C_3-C_{12}-H_{24}	159.003
C_{16}-O_{23}	1.397	C_3-C_{12}-H_{24}	110.5	C_2-C_3-C_{12}-O_{25}	35.608
C_{12}-H_{24}	1.081	C_3-C_{12}-O_{25}	110.6	C_3-C_{12}-O_{25}-C_{26}	157.646
C_{12}-O_{25}	1.395	C_{12}-O_{25}-C_{26}	114.8	C_{12}-O_{25}-C_{26}-O_{27}	179.212
O_{25}-C_{26}	1.327	O_{25}-C_{26}-O_{27}	105.6	O_{25}-C_{26}-O_{27}-C_{28}	179.833
C_{26}-O_{27}	1.285	C_{26}-O_{27}-C_{28}	117.1	C_{26}-O_{27}-C_{28}-H_{29}	120.585
O_{27}-C_{28}	1.42	O_{27}-C_{28}-H_{29}	107.9	C_{26}-O_{27}-C_{28}-H_{30}	-120.907
C_{28}-H_{29}	1.08	O_{27}-C_{28}-H_{30}	107.9	C_{26}-O_{27}-C_{28}-H_{31}	-0.136
C_{28}-H_{30}	1.08	O_{27}-C_{28}-H_{31}	110.1	O_{14}-C_{15}-C_{21}-H_{32}	-0.136
C_{28}-H_{31}	1.079	C_{15}-C_{21}-H_{32}	132.5	C_{15}-C_{21}-C_{22}-O_{33}	-177.656
C_{21}-H_{32}	1.067	C_{21}-C_{22}-O_{33}	129.8		
C_{22}-O_{33}	1.366				

Table 1: Optimized geometrical parameters of GMA at the DFT level.

Potential energy surface (PES)

Theoretical approaches to the link between the structure, energetics and dynamics of disordered materials demand computational techniques that are able to map the low energy portion of the potential energy surface accurately [13,14]. The PES scan for conformational motion of GMA molecule was constructed using energies after the optimization of stationary points geometries found at the DFT level. The calculated result shows that the global minimum energy of GMA was found to be -554437 kcal mol^{-1}. The torsion angle around the phenyl ring (C_2-C_3-C_{12}-C_{13}) with step angle of 10° is plotted in Figure 2.

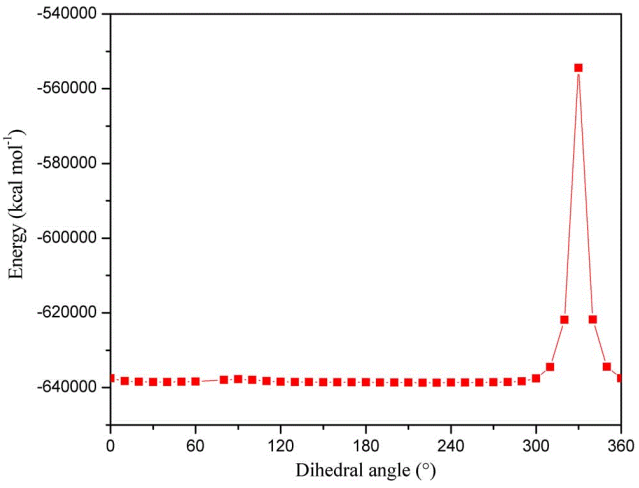

Figure 2: PES scan for dihedral angles C_2-C_3-C_{12}-C_{13} at DFT level.

NBO analysis

The NBO analysis is already proved to be an effective tool for chemical interpretation of hyperconjugative interaction and ED transfer from the filled lone pair orbital. The NBO calculations [15] were performed using NBO 3.1 program as implemented in the Gaussian 03 package in order to understand various second order interactions between the filled orbitals of one subsystem and vacant orbitals of another subsystem, which is a measure of the intermolecular delocalization or hyperconjugation. NBO analysis provides the most accurate possible 'natural Lewis structure' picture of single basis orbital j, because all orbital details are mathematically chosen to include the highest possible percentage of the electron density. The second order Fock matrix was carried out to evaluate the donor–acceptor interactions in the NBO basis [16]. For each donor (i) and acceptor (j), the stabilization energy E(2) associated with the delocalization i→j is estimated as

$$E(2) = \Delta E_{ij} = q_i \frac{F(i,j)^2}{\varepsilon_j - \varepsilon_i} (1)$$

Where qi is the donor orbital occupancy, εi and εj are diagonal elements and F(i,j) is the off diagonal NBO Fock matrix element.

Second-order perturbation theory analysis of Fock matrix in NBO basis, and the formation of Lewis and Non-Lewis orbitals by the valance hybrids corresponding to the intra-molecular C-H…O hydrogen bonds of GMA is given in Tables 3 and 4. The existence of intra-molecular hydrogen bonds due to the interaction between the lone pair of oxygen and anti-bonding orbitals of LP1O19 – σ*(C_4-H_9), LP_1O_{27} – σ *(C_{28}-H_{31}), LP_2O_{27} –σ *(C_{28}-H_{29}), LP_2O_{27} –σ *(C_{28}-H_{30}) have been confirmed by the NBO result. The strengthening and contraction of the C-H bonds is due to rehybridization [17], which is revealed by the low value of ED 0.01561, 0.018087, 0.01086 and 0.01572 e in the σ *(C_4-H_9), σ *(C_{28}-H_{31}), σ *(C_{28}-H_{29}) and σ *(C_{28}-H_{30}) orbitals respectively. The intramolecular C-H…O interactions are also evident from the hydrogen bonding geometry. The intramolecular contacts of O_{19}…H_9, O_{27}…H_{29}, O_{27}…H_{30}, and O_{27}…H_{31} are 2.566, 2.046, 2.045 and 2.122 Å, respectively, which are significantly shorter than the van der Waals separation between the O-H atom (2.73 Å) [18], indicating the possibility of intramolecular C-H…O interaction.

Donor NBO (i)	Acceptor NBO (j)	E(2)[a]	E(j)-E(i)[b]	F(i,j)[c]
		kJ/mol	a.u.	a.u.
LP1O_{19}	σ∗(C^4-H^9)	0.71	1.07	0.025
LP2 O_{19}	σ∗(C^{17}-H^{18})	2.3	0.79	0.038
LP1 O_{25}	σ∗(C^{12}-X^{24})	3.36	1.08	0.054
LP1 O_{27}	σ∗(C^{28}-X^{29})	3.24	0.74	0.047
LP2 O_{27}	σ∗(C^{28}-X^{30})	3.12	0.74	0.046
LP2 O_{27}	σ∗(C^{28}-X^{31})	3.6	0.99	0.054

[a]Energy of hyperconjugative interaction (stabilization energy).

[b]Energy difference between donor i and acceptor j NBO orb.

[c]Fock matrix element between i and j NBO orbitals.

Table 2: Second-order Perturbation theory analysis of Fock Matrix in NBO basis corresponding to the intramolecular C-H…O hydrogen bonds of GMA.

Bond (A-B)	ED/Energy (a.u)	ED_A%	ED_B%	NBO	s%	p%
σ(C_4-H_9)	1.98023	62.8	37.2	0.7925 ($sp^{2.37}$)$_C$	29.61	70.31
	-0.53363	-	-	+0.6099 (s)$_H$	-	-
σ∗(C_4-H_9)	0.01561	37.2	62.8	0.6099 ($sp^{2.37}$)$_C$	29.61	70.31
	0.43728	-	-	-0.7925 (s)$_H$	-	-
σ(C_{17}-H_{18})	1.92814	64.59	35.41	0.8037 ($sp^{2.96}$)$_C$	25.22	74.69
	-0.57133	-	-	+0.5950($sp^{1.33}$)$_H$	-	-
σ∗(C_{17}-H_{18})	0.02534	35.41	64.59	0.5950 ($sp^{2.96}$)$_C$	25.22	74.69
	0.44529	-	-	-0.8037 (s)$_H$	-	-
σ(C_{127}–H_{24})	1.95357	64.19	35.81	0.8012 ($sp^{2.88}$)$_C$	25.73	74.18
	-0.56755	-	-	+0.5984 ($sp^{1.33}$)$_H$	-	-
σ∗(C_{12}-H_{24})	0.0328	35.81	64.19	0.5950 ($sp^{2.88}$)$_C$	25.73	74.18
	0.4647	-	-	-0.8037 (s)$_H$	-	-
σ(C_{28}-H_{29})	1.99184	61.51	38.49	0.7843 ($sp^{2.80}$)$_C$	26.26	73.64
	-0.53665	-	-	+0.6065 (s)$_H$	-	-
σ∗(C_{28}-H_{29})	0.01087	38.49	61.51	0.6065 ($sp^{2.80}$)$_C$	26.26	73.64
	0.39798	-	-	-0.7843 (s)$_H$	-	-
σ1(C_{28}-H_{30})	1.99194	61.46	38.54	0.7840 ($sp^{2.81}$)$_C$	26.23	73.67
	-0.53688	-		+0.6208 (s)$_H$	-	-
σ1∗(C_{28}-H_{30})	0.01086	38.54	61.46	0.6208 ($sp^{3.68}$)$_C$	26.23	73.67
	0.3975	-	-	-0.7840 (s)$_H$	-	-

$\sigma 2(C_{28}\text{-}H_{31})$	1.99725	61.91	38.09	0.7868 $(sp^{2.59})_C$	27.80	72.1
	-0.54251	-	-	+0.6172 $(s)_H$	-	-
$\sigma 2*(C_{28}\text{-}H_{31})$	0.01572	38.09	61.91	0.6172 $(sp^{99.99})_C$	27.80	72.1
	0.39704	-	-	-0.7868 $(s)_H$	-	-
$LP_1\ O_{19}$	1.97476	-	-	$(sp^{1.07})o$	48.19	51.74
	-0.63434				-	-
$LP_2\ O_{19}$	1.94696	-	-	$(sp^{1.00})o$	0.01	99.88
	-0.34228				-	-
$LP_1\ O_{25}$	1.70945	-	-	$(sp^{1.00})o$	0	99.85
	-0.61129				-	-
$LP_1\ O_{27}$	1.96807	-	-	$(sp^{1.52})o$	39.57	60.34
	-0.59419				-	-
$LP_2\ O_{27}$	1.7294	-	-	$(sp^{1.00})o$	0	99.84
	-0.34262				-	-

Table 3: NBO result showing the formation of Lewis and Non-Lewis orbitals by the valance hybrids corresponding to the intramolecular C-H…O

Vibrational spectral analysis

The analysis of the vibrational spectra is based on the FT-IR spectrum and the vibrational wavenumbers computed at the B3LYP/6-31G(d) level with their scaled value. The calculated vibrational wavenumbers, measured infrared band positions and their tentative assignments are presented in Table 4. The observed and simulated FT-IR spectra of GMA are given in Figure 3. The vibrational analysis was performed on the basis of the characteristic vibrations of hydroxyl, carbonyl, phenyl, and methyl group.

Hydroxyl vibration: The hydroxyl groups are likely to be the most sensitive to the environment and so they show pronounced shifts in the spectrum of the hydrogen bonded species. The hydroxyl group absorbs strongly in the 3700-3584 cm^{-1} region, whereas the existence of intermolecular hydrogen bond formation can lower the O-H stretching wavenumber to 3550-3200 cm^{-1} region [19,20]. The IR spectrum in the high region shows a broad intense band at 3537 cm^{-1}attributed to hydrogen-bonded OH stretching. The in-plane OH deformation vibration usually appears as a strong band in the region 1440-1260 cm^{-1} [21]. The medium band at 1379 cm-1 corresponds to the in-plane bending mode of the hydroxyl vibration. The OH out of plane deformation vibration lies in the 290-320 cm-1 for free OH and in the region 517-710 cm^{-1} for associated OH [22]. The medium band at 698 cm^{-1} corresponds to out-of-plane bending vibration of hydroxyl group.

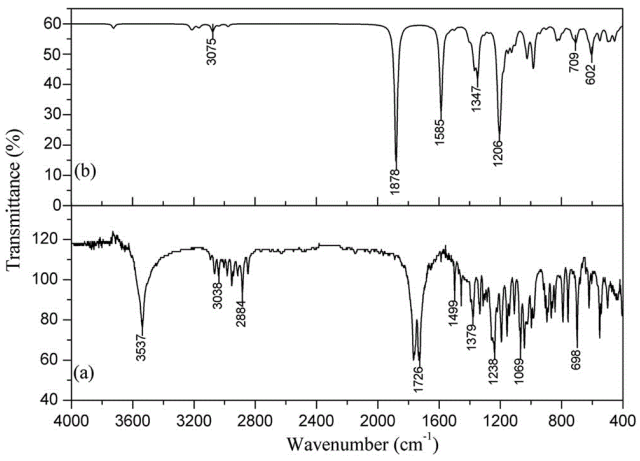

Figure 3: (a) FT-IR spectra of GMA (b) Simulated IR spectra of GMA.

ν_{IR} (cm^{-1})	ν_{cal} (cm^{-1})	IR Intensity	Assignment
3537 m	3580	29.3	O_{19}-H_2O stretch
3094 w	3098	7.4	C-H stretch 2 of Ph ring
3065 w	3081	14.5	C-H stretch 20a of Ph ring
3007 w	3040	16.7	CH_3 asym. stretch
2947m	2957	51.8	CH_3 sym. stretch
2920 w	2918	10.2	C_{12}-H_{24} stretch
2884 w	2861	17	C_{17}-H_{18} stretch
1770 s	1807	927	C_{22}=O_{33} stretch
1605 w	1594	4.3	C-C stretch 8a of Ph ring
1588 w	1582	2.3	C-C stretch 8b of Ph ring +C_{12}-H_{24} ipb
1490 w	1484	13.7	C-C stretch 19a of Ph ring
1459 w	1459	3.8	CH_3 asym. bend
1418 w	1437	13.8	CH_3 umbrella mode
1394 w	1411	2.9	C_{21}-C_{16}-C_{15} stretch+C_{13}-O_{14} stretch
1379 m	1350	66.3	C_{12}-H_{24}, C_{17}-H_{18}, C_{21}-H_{32} ipb +O_{19}-H_{20} bend+C-H ipb 3 of Ph ring+CH_3 umbrella
1342 w sh	1337	27.4	C_{12}-H_{24} ipb+O_{19}-H_{20} bend+C-H ipb 3 of Ph ring
1329 w	1321	14.8	C-H ipb 3 of Ph ring+O_{19}-H_{20} ipb
1310 w	1311	18.9	C_{12}-H_{24}, C_{17}-H_{18} ipb+O_{19}-H_{20} ipb+C-C stretch 14 of Ph ring

1305 w	1309	28.8	C_{12}-H_{24}, C_{17}-H_{18} ipb+O_{19}-H_{20} ipb+C-C stretch 14 of Ph ring
1283 w	1294	297.4	C12-H24 ipb +C28-H31 ipb +O19-H20 ipb+C-C stretch 14 of Ph ring
1256 m sh	1253	30.6	C_{12}-H_{24}, C_{17}-H_{18}, C_{21}-H_{32} ipb +O_{19}-H_{20} bend+C-C stretch 14 of Ph ring
1238 m	1226	19	C_{12}-H_{24}, C_{17}-H_{18}, C_{21}-H_{32} ipb +O_{19}-H_{20} bend+C-H ipb 3 of Ph ring
1194 m	1171	9	C_{12}-H_{24}, C_{17}-H_{18}, C_{21}-H_{32} ipb +O_{19}-H_{20} bend
1153 m	1155	469.8	C-H ipb 18a of ph ring
1142 w	1147	2	CH_3 opb
1105 m	1104	107.4	C_{12}-H_{24}, C_{17}-H_{18}, C_{21}-H_{32} ipb +O_{19}-H_{20} bend
1081 msh	1081	117.8	C-H ipb 15 of Ph ring+C_{12}-H_{24} ipb
1069 m	1064	28.4	C-H ipb 15 of Ph ring+C_{12}-H_{24} ipb
1041 m	1058	68.4	C_{17}-H_{18}, C_{21}-H_{32} ipb
1027 w	1018	4.7	C-C radial skeletal 12 of Ph ring
998 w	999	40.6	C_{12}-H_{24}, C_{17}-H_{18} ipb
985 w	985	181.4	C_{12}-O_{25},C_{28}-O_{27} stretch
921 vw	940	7.3	C-H opb 17a of Ph ring
791 w	781	71.8	C-H opb 10b of Ph ring
751 w	759	29.5	C-H opb 10b of Ph ring
698 m	698	59.1	C-H opb 11of Ph ring+OH opb
623 w	609	3.5	OpSkeletal 6b of Ph ring
604 vw	603	45	OpSkeletal 6b of Ph ring
548 m	578	147.1	C_{12}-H_{24}, C_{17}-H_{18} opb
535 m	528	91.2	OpSkeletal 6b of Ph ring +C_{13}-O_{14}-C_{15} bend
419 w	436	93.5	C_{12}-O_{25}-C_{26}, C_{26}-O_{27}-C_{28}, C_{16}-O_{22}-C_{24} bend
407 w	411	20.7	C_{12}-O_{25}-C_{26},C_{26}-O_{27}-C_{28} bend

Table 4: FT-IR and calculated vibrational wavenumbers, infrared intensities and assignment for GMA.

Carbonyl vibration: Carbonyl group vibrations in ketones are the best characteristic bands in the vibrational spectra, and for this reason, such bands have been the subject of extensive studies [23]. The carbonyl stretching vibrations of ketones have normally strong intensity and are expected in the region 1715-1680 cm^{-1} [24]. In GMA the carbonyl vibration C_{22}=O_{33} stretch is calculated as 1807 $cm^{-1}$and is observed at 1770 cm^{-1} as a strong intensity. This higher wavenumber 1770 cm^{-1} indicates the stretching vibration of C=O bond is not interacting with other atoms in the vicinity of the ring. The C_{13}-O_{14} stretch is calculated as 1411 $cm^{-1}$and is observed at 1394 cm^{-1} as a weak intensity. Normally the C-O-C bending vibration is expected in the region around 440 cm^{-1}. In GMA the C_{12}-O_{25}-C_{26}, C_{26}-O_{27}-C_{28}, C_{16}-O_{22}-C_{24} bending is observed as a weak band at 419 cm^{-1}.

Phenyl ring vibration: The various normal vibrations of the monosubstituted benzene ring are assigned according to Wilson's numbering convention [25]. Of the five allowed C-H stretching modes 2, 20a, 20b, 7a and 7b for the mono substituted ring, 2 and 20a are found to be active. The C-H stretching vibration appears to be very weak, which is due to the charge carrier localization in the phenyl ring [26]. The weak bands observed at 3094 and 3065 cm^{-1} are assigned for mode 2, 20a, respectively. Normal vibrations 8a, 8b, 19a, 19b and 14 are classified as the C-C stretching vibrations of the monosubstituted rings. The normal mode 8a has been observed at 1605 cm^{-1} as a weak intensity and is calculated at 1594 cm^{-1}. The weak band observed at 1588 cm^{-1} in IR is assigned to 8b mode. The 19a mode in monosubstituted ring can be expected near 1500 cm^{-1} as a stronger band and 19b appear as a weak band around 1470 cm^{-1} [25]. The weak band observed at 1490 cm^{-1}in is due to contribution of 19a mode. The C-C stretching mode 14 is observed as a medium shoulder band at 1256 cm^{-1} which is attributed to the isotopic effect of the carbon.

Normal vibration 3, 9a, 15, 18a and 18b are classified as C-H in-plane bending vibrations of monosubstituted phenyl rings. Mode 3 is coupled with O-H in-plane bending, methane in-plane bending and methyl deformation, which are observed as a series of bands at 1379, 1342, 1329 cm^{-1}. The higher intensity of the IR band at 1379 cm^{-1} is due to the contribution of the methyl umbrella mode [27]. The intense band at 1153 cm^{-1} is assigned to the mode 18a and is calculated to be 1155 cm^{-1}. The C-H in-plane bending mode 15 is observed at 1081 and 1069 cm^{-1} as a medium intensity which is coupled with methane bending.

The absorption bands arising from the C-H out-of-plane vibrations are usually observed in the region 1000-675 cm^{-1} [28]. Although the allowed C-H out of plane modes are 5/10b, 11/17b, 10a and 17 a, only the modes 17a, 10b and 11 are active for GMA. The mode 17a is observed in IR at 921 cm^{-1} as a very weak intensity. The weak intense bands in IR at 751 and 698 cm^{-1} are assigned for C-H out of plane bending modes 10 and 11. The in-plane ring deformations derived from the b1u benzene vibration 12 gives rise to an intense band in monosubstituted benzene [29] at 1010-990 cm^{-1}. The radial skeletal vibration 12 of GMA is observed as weak band at 1027 cm^{-1} and the ring deformation 6b is observed as a weak band at 604 cm^{-1}.

Methyl group vibration: The asymmetric C-H stretching mode of CH_3 is expected around the region 2980 cm^{-1} and the symmetric one is expected in the region 2870 cm^{-1}[19,30]. The CH_3 asymmetric stretching vibration appears as a weak band at 3007 cm^{-1}. The symmetric stretching mode is observed as a medium intense band at 2947 cm^{-1}. The shifting of higher wavenumber in the IR spectrum is due to the influence of electronic effect resulting from hyperconjugation and induction of methyl group with the aromatic ring system. The asymmetric and symmetric bending vibrations of methyl groups normally appears in the region 1465-1440 cm^{-1} and 1390-1370 cm^{-1}, respectively, [21,28]. The weak band at 1418 cm^{-1} in the infrared spectrum is attributed to the CH_3 asymmetric bending, and the weak band at 1418 cm^{-1} is assigned to the CH_3 symmetric bending mode.

Thermo dynamical parameters

Thermodynamic properties, such as heat of formation (HOF), enthalpy and entropy, are important parameters to evaluate the explosive properties of an energetic compound. For stable compounds, of course, there are many tables that contain experimental data. However, for energetic materials and unstable compounds, determination of the thermodynamic properties is impractical or dangerous. At the present time one may calculate them from empirical models such as group additive methods. Such methods work very well for hydrocarbons, but often fail for other classes of compounds [31]. The HF and DFT levels calculated thermodynamic parameters are presented in Table 5. Scale factors have been recommended [32] for an accurate prediction in determining the zero-point vibration energies (ZPVE) and the entropy S. The variations in the ZPVE s seem to be insignificant. The total energies are found to decrease with the increase of the basis set dimension. The changes in the total entropy of BMP at room temperature at different basis sets are only marginal.

Parameters / **Calculated level**	**HF/6-31G(d)**	**B3LYP/6-31G(d)**
Total energy	-2688386.937	-2704071.565
Zero-point energy	165.83582	152.21554
Rotational constants	0.34773	0.36441
	0.23026	0.2062
	0.16578	0.15388
Entropy	-	-
Total	64.188	70.824
Rotational	2.981	2.981
Translational	2.981	2.981
Vibrational	58.226	64.862
Dipole moment	11.9847	9.4911

Table 5: Theoretically computed total energies (kJ mol^{-1}) zero-point vibrational energies (kcal mol^{-1}), rotational constants (GHz), entropies (cal mol^{-1} K^{-1}) and dipole moments (debye) for GMA.

Molecular orbitals

One property of the electronic structure that changes in a consistent manner for a wide variety of chemical reactions is the difference in energies between the highest occupied molecular orbital (HOMO) and the LUMO, the HOMO–LUMO gap. For many reactions involving the interaction of these two orbitals the value of the HOMO–LUMO gap is a minimum at, or near, the transition state [33].The electronic structures of Goniofufurone monoacetate, have been analyzed with B3LYP/6-31 G(d) level. The delocalized molecular structure HOMO, HOMO-1, HOMO-2 and LUMO, LUMO+1, LUMO+2 of GMA are plotted in Figure 4. From the figure HOMO of GMA is delocalized on π orbitals of the lactone ring. The reported HOMOs have a bonding π character, that the HOMO and HOMO-2 show a partial non-bonding character due to the carboxylic oxygen lone pair. The LUMOs have antibonding π* character and are highly delocalized over the whole molecules, all the LUMOs show more charge delocalization on the benzene ring.

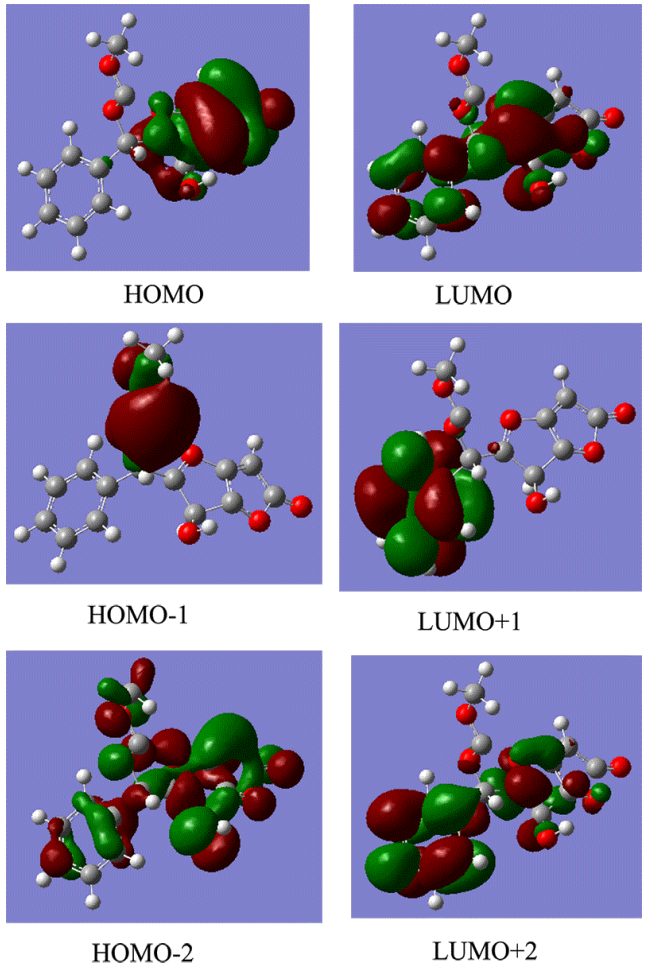

Figure 4: The delocalized molecular structure of GMA.

Conclusion

The understanding of the structure–property correlation of Goniofufurone monoacetate (GMA) materials is important for the development of pharmacological drug materials. The structural features of the highly efficient pharmacological drug GMA as well as the vibrational spectral investigations have been carried out from FT-IR spectra aided by the DFT computations. The vibrational analysis of GMA was performed using DFT calculations. From the optimized geometry the torsion angles C_{15}-C_{16}-C_{21}-O_{23} = 6.9125°, C_{15}-C_{21}-C_{22}-O_{23} = 2.6337° show that the five-membered lactone ring adopts the 2E conformation. The blue shifting of CH_3 symmetric stretching mode in the IR spectrum is due to influence of electronic effect resulting from hyperconjugation and induction of methyl group with the aromatic ring system. NBO analysis confirms the C-H...O intramolecular hydrogen bonding. The calculated HOMO-LUMO energy was comparatively low and it substantiates the possibility of the intramolecular charge delocalization. These charge delocalization stimulate the pharmaceutical property in the molecule.

Acknowledgement

Authors B. R. K, M. D. A and G. J are thankful to KSCSTE, Govt. of Kerala for financial assistance.

References

1. Hisham A, Toubi M, Shuaily W, Ajithabai MD, Fujimoto Y (2003) Cardiobutanolide, a styryllactone from goniothalamus cardiopetalus. Phytochemistry 62: 597-600.
2. Harikumar B, BabuVarghese, Jayakumar G, Ajithabai M.D (2006) 4.8-hydroxy-7-phenyl-2,6-dioxabicyclo[3.3.1]nonan-3-one. Acta Cryst E62: 5567-5570.
3. Xin-ping F, Anderson Jon E, Ching-jer chang, Philip E Fanwick, Jerry L McLaughlin (1990) Novel bioactive styryl-lactones: goniofufurone, goniopypyrone, and 8-acetylgoniotriol from Goniothalamus giganteus(annonaceae). X-Ray molecular structure of goniofufurone and of goniopypyrone. J Chem Soc Perkin Trans 1: 1655-1661.
4. Zhang YJ, Zhou GX, Chen RY, Yu DQ (1999) Styryllactones from the rhizomes of Goniothalamus griffithii. J. Asian Nat Prod Res. 1: 189-197.
5. Rosskopf F, Kraus J, Franz G (1992) Immunological and antitumor effects of coumarin and some derivatives. Pharmazie 47:139-142.
6. Nam SI, Min ES, Jung YM, Lee MS (2001) Fermi Resonance and Solvent Dependence of the νC=O Frequency Shifts of Raman Spectra: Cyclohexanone and 2-Cyclohexen-1-one. Bull. Korean Chem. Soc. 22: 989-993.
7. Frisch MJ, Trucks GW (2009) Gaussian-09, Revision A.02, Gaussian, Inc., Wallingford CT.
8. Becke AD (1993) Density-functional thermochemistry. III. The role of exact exchange. J Chem Phys 98: 5648-5652.
9. Lee CT, Yang WT, Parr RG (1988) Development of the Colle-Salvetti Correlation-energy formula into a functional of the electron density. Phys Rev B 37: 785-789.
10. Ravikumar C, Hubert Joe I, Jayakumar V.S (2008) Charge transfer interactions and nonlinear optical properties of push–pull chromophore benzaldehyde phenylhydrazone: a vibrational approach. Chem Phys Lett 460: 552-558.
11. Scott AP, Random L (1996) Harmonic Vibrational Frequencies: An Evaluation of Hartree-Fock, Moller-Plesset, Quadratic Configuration Interaction, Density Functional Theory, and Semiempirical Scale Factor. J Phys Chem 100: 16502-16504.
12. Vratislav L, Dalma G, Marian K, Peter K, Matej, et al. (2003) Preparation and Crystal Structure of (1S, 5S, 7S, 8R)-8-Hydroxy-7-phenyl-2,6-dioxabicyclo[3.3.0]octan-3-one. Molecules 8: 599-606.
13. Bosenick A, Dove MT, Mayers ER, Palin EJ, Sainz-Daiz CI, et al. (2001) Computational methods for the study of energies of cation distributions: applications to cation-ordering phase transitions and solid solutions. Mineral Mag 65: 193-199.
14. Bakken E, Allan NL, Barron THK, Mhon CE, Todorov IT, et al. (2003) Order-disorder in grossly non-stoichiometric SrFeO 2.50-a simulation study. Chem Chem Phys 5: 2237-2243.
15. Glendening ED, Badenhoop JK, Reed AE, Carpenter JE, Bohmann JA, et al. (2001) NBO 5.0, Theoretical Chemistry Institute, University of Wisconsin, Madison.
16. Reed AE, Curtiss LA, Weinhold F (1988) Intermolecular Interactions from a Natural Bond Orbital, Donor-Acceptor Viewpoint. Chem Rev 88: 899-926.
17. Alabugin IV, Manoharan M, Peabody S, Weinhold F (2003) Electronic basis of improper hydrogen bonding: a subtle balance of hyperconjugation and rehybridization. J Am Chem 125: 5973-5987.
18. Sato H, Dubal J, Murakami R, Noda I, Ozaki Y (2005) Infrared and Raman spectroscopy and quantum chemistry calculation studies of C–H O hydrogen bondings and thermal behavior of biodegradable polyhydroxyalkanoate. J Mol Struct 744: 35-46.
19. Smith BC (1999) Infrared Spectral Interpretation, A Systematic Approach, CRC Press, Washington, DC.
20. Silverstein RM, Webster FX (2003) Spectroscopic Identification of Organic Compounds (6th edn.) John Wiley & Sons, New York.
21. Socrates G (1980) Infrared Characteristic Group Frequencies (3rd edn.) John Wiley& Sons, New York.
22. Varsanyi G (1974) Assignments for Vibrational Spectra of Seven Hundred Benzene Derivatives, Science, Academic Kiaclo 2.
23. Sajan D, Binoy J, Pradeep B, Venkta Krishna K, Kartha VB, et al. (2004) NIR-FT Raman and infrared spectra and ab initio computations of glycinium oxalate. Spectrochim Acta 60A: 174-180.
24. Bellamy LJ (1980) The infrared spectra of Complex Molecules, Chapmann and Hall, London.
25. Amalanathan M, Cinta Pinzaru S, Hubert Joe I, Irena Kostova, Ravikumar C (2009) Theoretical and vibrational spectral investigation of sodium salt of Acenocoumarol. J Raman Spectrosc 40:1033-1038.
26. Neugebauer H, Kvarnstrom C, Brabec C, Sariciftci NS, Kiebooms R, et al. (1999) Infrared spectroelectrochemical investigations on the doping of soluble poly(isothianaphthene methine) (PIM). J Chem Phys 110: 12108-12112.
27. James C, Amal Raj A, Reghunathan R, Jayakumar VS, Hubert Joe I (2006) Structural conformation and vibrational spectroscopic studies of 2,6-bis (p-N,N-dimethyl benzylidene) cyclohexanone using density functional theory. J Raman Spectrosc 37: 1381-1392.
28. Colthup NB, Daly LH, Wiberley SE (1990) Introduction to Infrared and Raman Spectroscopy, Academic Press, New York.
29. Dollish FR, Fateley WG, Bentley FF (1997) Characteristic Raman Frequencies of Organic Compounds, John Wiley & sons, New York.
30. Kleinman DA (1962) Phys Rev 126: 1977-1982.
31. Dixon DA, Smart BE (1990) Numerical Simulation of Molecular Systems. The Determination of Thermochemical Properties. Chem Eng Commun 98: 173-185.
32. Alcolea PM (2000) Scaling factors for the prediction of vibrational spectra. I. Benzene molecule. Int J Quantum Chem 77: 661-684.
33. Bader RFW (1962) Vibrationally induced perturbations in molecular electron distributions. Can J Chem 40: 1164-1175.